

## Article

# Fault Activity in Clay Rock Site Candidate of High Level Radioactive Waste Repository, Tamusu, Inner Mongolia

Zheng Rao <sup>1</sup>, Guangrong Li <sup>1,\*</sup>, Xiaodong Liu <sup>1,2</sup>, Pinghui Liu <sup>1</sup>, Honghui Li <sup>3</sup>, Shuai Liu <sup>1</sup>, Minqiang Zhu <sup>1</sup>, Chao Guo <sup>1</sup>, Fengjuan Ni <sup>1</sup>, Zhijun Gong <sup>1</sup> and Fiaz Asghar <sup>1</sup>

<sup>1</sup> State Key Laboratory of Nuclear Resources and Environment, East China University of Technology, Nanchang 330013, China; 201800818014@ecut.edu.cn (Z.R.); 198260003@ecut.edu.cn (X.L.); 199560031@ecut.edu.cn (P.L.); 200360016@ecut.edu.cn (S.L.); Zhumq@ecut.edu.cn (M.Z.); 2016070945@ecut.edu.cn (C.G.); 202062003@ecut.edu.cn (F.N.); 201660006@ecut.edu.cn (Z.G.); L2017008103@ecut.edu.cn (F.A.)

<sup>2</sup> Jiujiang University, Jiujiang 332005, China

<sup>3</sup> China Institute for Radiation Protection, Taiyuan 030006, China; lihonghui@cirp.org.cn

\* Correspondence: liguangrong0086@ecut.edu.cn

**Abstract:** Tamusu area in Inner Mongolia is one of the favorable site candidates for high level radioactive waste (HLW) repository, which requires a stable regional tectonic environment. Field investigation, mossbauer spectroscopy, major elements, carbon and oxygen isotope and quartz micro morphology of fault gouge and host rock of three faults in the site candidate were conducted. The results show that the F<sub>2</sub> and F<sub>7</sub> faults on the north and south sides of the site candidate are in a relatively stable state with good sealing and weak activity. Part of the F<sub>4</sub> fault is located in the site candidate, and the deportment of a small amount of pyrite in the fault zone and the difference of carbon and oxygen isotopes indicate that it may have experienced material exchange with the deep zone. Attention should be paid to induced earthquake risk.

**Keywords:** Tamusu; clay rock; geological repository; fault activity; high level radioactive waste



**Citation:** Rao, Z.; Li, G.; Liu, X.; Liu, P.; Li, H.; Liu, S.; Zhu, M.; Guo, C.; Ni, F.; Gong, Z.; et al. Fault Activity in Clay Rock Site Candidate of High Level Radioactive Waste Repository, Tamusu, Inner Mongolia. *Minerals* **2021**, *11*, 941. <https://doi.org/10.3390/min11090941>

Academic Editor: Tsutomu Sato

Received: 11 July 2021

Accepted: 20 August 2021

Published: 29 August 2021

**Publisher's Note:** MDPI stays neutral with regard to jurisdictional claims in published maps and institutional affiliations.



**Copyright:** © 2021 by the authors. Licensee MDPI, Basel, Switzerland. This article is an open access article distributed under the terms and conditions of the Creative Commons Attribution (CC BY) license (<https://creativecommons.org/licenses/by/4.0/>).

## 1. Introduction

With the rapid development of China's nuclear energy industry, how to safely and effectively dispose HLW will become an urgent issue. After years of practice and research, the safest and most effective method of disposal for HLW is deep geological disposal, which has been widely recognized by various countries in the world and many international organizations such as the International Atomic Energy Agency (IAEA). The site selection of the repository is particularly important for the disposal of HLW, and social factors and natural factors need to be considered. Among them, the stability of regional structure is a very important aspect of natural factors.

Igneous crystalline and volcanic rocks, argillaceous clay rocks and salts are usually chosen as host rock for deep geological disposal [1]. Compared with granite, clay rock has the characteristics of low permeability, strong ability to block the migration of radionuclides and good self-sealing [2,3]. The site candidate of Tamusu in Inner Mongolia can meet the requirements of geological conditions, environmental protection, land use, social impact and waste transportation for HLW disposal, and can be used as one of the favorable site candidate for HLW repository. However, the faults developed in this area may have potential risk to repository.

Multi-stage fault activity or fault activity under strong stress may cause material fragmentation or even mud pulverization in the fault zone, so, the study of fault activity is an important aspect of safety evaluation for deep geological disposal of HLW. Fault gouge is usually a direct product of fluid-rock interaction and fault activity [4]. Studies have shown that the distribution of iron species in fault gouge can indicate the oxidation–reduction

environment of the fault zone [5]. The characteristics of major elements in fault gouge would suggest the degree of fluid-rock interaction in fault zone and reflect the intensity of fault activity [6–8]. The isotope distribution characteristics in the fault gouge can indicate the fluid source of the fluid-rock interaction in the fault zone [9]. The micro morphology of quartz grains in fault gouge can also give information on active age and movement mode of faults [10]. Therefore, fault gouge contains a variety of important information of fault activity [11,12], which is of great significance for understanding the stability of regional geological bodies. Herein, the multi technologies have been applied to the Tamusu candidate to study the fault activities.

## 2. Geological Setting

### 2.1. Tectonic Setting

Bayingebi basin, which resulted from Paleozoic plate continent-continent collision, namely the result of convergence of Tarim plate, Kazakhstan plate, Siberian plate and North China plate. Precisely, Bayingebi basin is a Meso Cenozoic sedimentary basin controlled by Altun strike-slip fault [13,14]. After experiencing the Paleozoic continent-continent collision and Mesozoic strike-slip pull-off evolution process, the basin as a whole is distributed in a near EW direction. The basin is divided into northern depression and southern depression by Zongnaishan-Shalazhashan uplift. The northern depression includes three sub-depressions: Chagandesu depression, Suhongtu depression and Guaizihu depression; the southern depression includes Yingen depression and Yingejing depression.

The Tamusu site candidate is located in the Yingejing depression of the Bayingebi basin. Geomorphically, the Yingejing depression shows NE extension with stable sedimentation, small phase change and large thickness. The faults in this depression are mainly NE, near EW or NW (Figure 1), and the fold structures are not developed [15].

### 2.2. Tectonic Characteristics

The Tamusu site candidate is located between the western segment of Zongnaishan-Shalazhashan uplift and Badanjin fault zone on the northern margin of Alxa block, where many faults develop (Figure 1).

Tamusu fault ( $F_2$ ) is located in the northern Tamusu, close to the basin-control fault ( $F_1$ ). It is a large concealed fault located in the piedmont sloping plain, with a length of about 40 km, strike of NE 70 degrees, and dip to Southeast with angle of 70~80 degrees (Figure 1). The Middle Jurassic strata in the western segment of the Tamusu fault ( $F_2$ ) thrusts over the lower Cretaceous Bayingebi Formation. Outcrop with drag trace in the lower Bayingebi Formation indicates weak left lateral torsion. Tamusu fault ( $F_2$ ) is a compressive fault.

Wulantiebuke fault ( $F_4$ ) is a concealed fault with length about 65 km, and the western segment of the fault is NE trending. From Wulantiebuke to Wulan Tolgoi, it gradually turns to about 90 degrees to the east. Most sections of the fault are covered by Quaternary strata, and only lower Cretaceous strata is limited exposed. This fault leads to upper and lower the lower Cretaceous Bayingebi Formation contact via fault locally. Wulantiebuke fault ( $F_4$ ) mostly developed in the lower Bayingebi Formation with rock fracture zone, along which most rocks are carbonated. The macroscopic geomorphological features of the fault suggest that it is a compressive fault.

The Narenhala fault ( $F_7$ ) is located in the area of Hulesitogoihudug-Narenhalashan-Tabutolgoi, with a total length of more than 250 km and strike of nearly 75 degrees NE. The fault divides the Yingejing depression into two parts, and is mostly covered by the Upper Cretaceous red beds and the Quaternary strata. The whole fault is a large arc-shaped concealed fault protruding to the south, and the modern landform is beaded saline-alkali land.

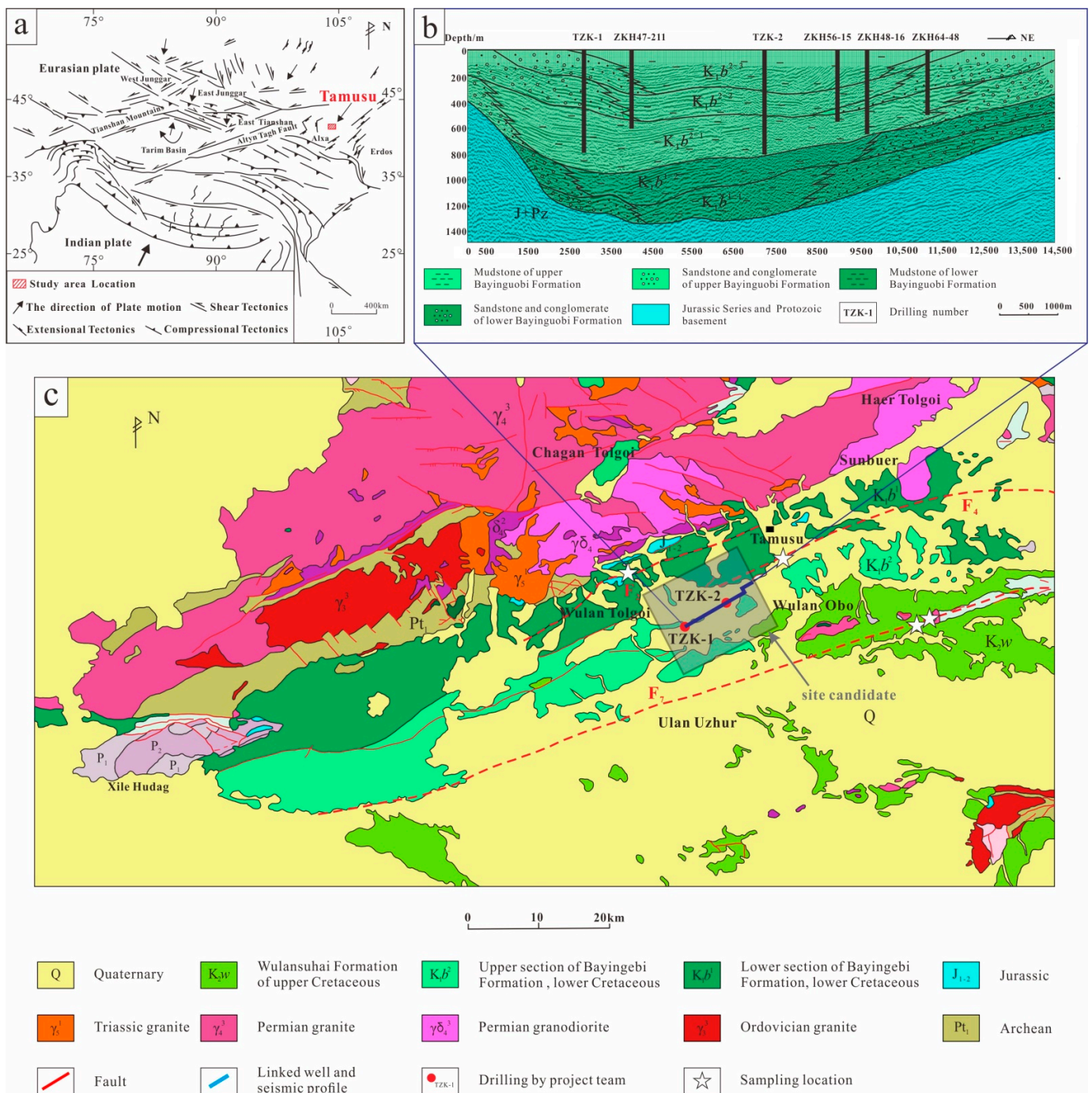


**Figure 1.** Deformation system of the Tibetan plateau type in west China and tectonic system map of Tamusu area. (a) shows the deformation system of Qinghai-Tibet Plateau in Western China, in which the red square shows the location of Tamusu study area; (b) is a near East-West holes-seismic profile in the candidate in (c); (c) shows the geological map of Tamusu study area.

### 3. Sample Collection and Analysis

The Tamusu site candidate is located between  $F_2$  and  $F_7$  faults, and part of the  $F_4$  fault is located in the site. The activity of fault highly affects the regional geological stability of the site candidate.

#### 3.1. Sample Collection

9 samples were collected from the three faults, including 4 host rock and 5 gouge samples. Detailed information is as following.

### 3.1.1. Samples from Tamusu Fault (F<sub>2</sub>)

There is no fresh outcrop in the middle and east sections of the Tamusu fault, but exposures in the west section. From the outcrop of the fault, the Longfengshan Formation of Jurassic is thrust over the upper member of Bayingebi Formation of Lower Cretaceous, the lithology is dominated by medium—coarse sandstone, and the color is yellowish-brown (Figure 2a,b). Gneissic granodiorite is outcropped locally on both sides of the fault cut by granite veins. The host rocks are relatively fragmented, and the joints are well developed. The sampled location mainly composed of yellowish fault gouge with small amount of breccia, and no structural lens or folded rocks is observed. The outcrop of fault gouge varies from 30 to 50 cm, and the clay content is uneven.

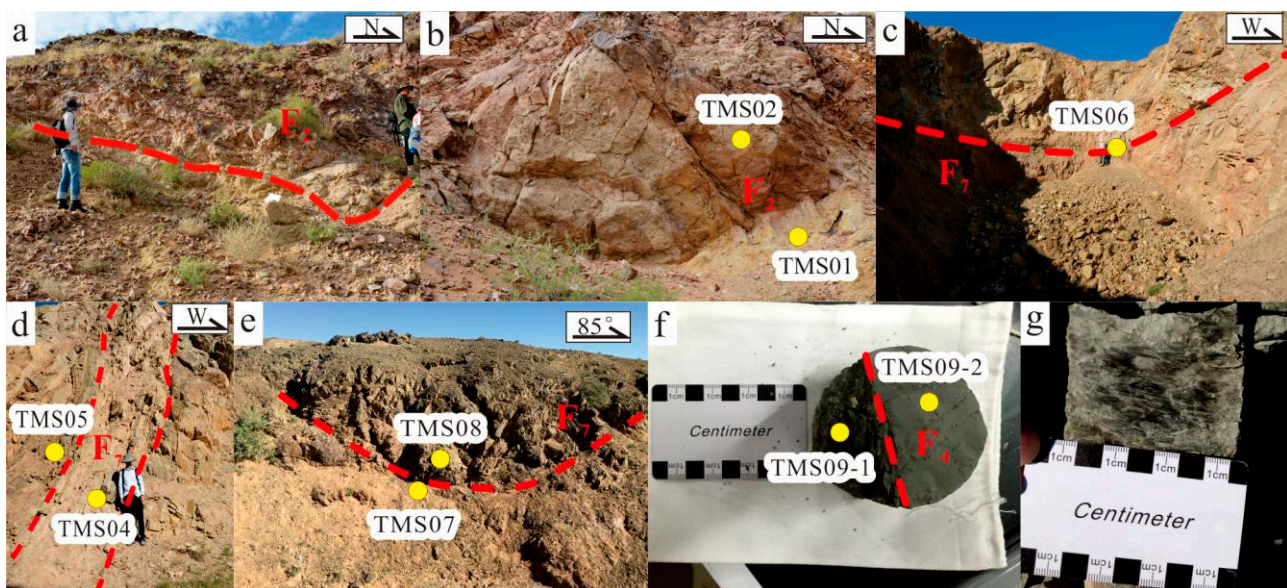


**Figure 2.** Field outcrops and sampling sites of faults. (a) western outcrop of F<sub>2</sub> fault; (b) F<sub>2</sub> fault sampling location; (c) F<sub>7</sub> fault outcrop one sampling location one; (d) F<sub>7</sub> fault outcrop one sampling location two; (e) F<sub>7</sub> fault outcrop two sampling location; (f) F<sub>4</sub> fault samples in drilling core; (g) contact surface between fault gouge and host rock of F<sub>4</sub> fault.

### 3.1.2. Samples from Wulantiebuke Fault (F<sub>4</sub>)

There is no outcrop on the surface, and the sample is collected from the core at the depth of 81 m. The core shows that the fault gouge is gray-black (Figure 2f) and contains small amount of breccia, and there is no ductile deformation. Cleavage is developed in the host rock near the fault gouge, and striation can be seen at the contact part between the fault gouge and the host rock (Figure 2g).

### 3.1.3. Samples from Narenhala Fault (F<sub>7</sub>)

The fault developed grayish-white to grayish-black fault gouge (Figure 2c,d) with thickness of about 50 cm small amount of breccia, and no structural lens and folds. In Figure 2e, two secondary faults intersect each other and are exposed near the surface. The clay content of fault gouge in different parts is quite varied. Calcite vein with thickness of about 10 cm is developed in fault gouge. The host rocks on both sides of the fault are seriously fractured, the joints are extremely developed. Moreover, 5 cm-thickness fault gouge with breccia is occasionally developed.

The samples of fault gouge and host rock were collected at the fault center of F<sub>2</sub> and F<sub>7</sub> faults, and about 20 cm of weathered rock and soil on the surface were removed before sampling. For F<sub>4</sub>, fault gouge and host rock samples were collected from the core in the depth of 81 m. The sampling locations are shown in Table S1. Fresh fault gouge samples were collected, packed in sealed plastic bags and transported back to the laboratory for analysis and treatment as soon as possible.

### 3.2. Analysis Method

#### 3.2.1. Quartz Micro Morphology

The observation of the micro morphology of quartz was completed in the field emission scanning electron microscope (Nova nanosem 450) of the State Key Laboratory of nuclear resources and environment, East China University of Technology (Nanchang, China). This microscope is equipped with the X-Max50X energy dispersive spectrometer (EDS) produced by Oxford Instruments Company (Oxford, UK). Before observation and statistics, the pure quartz grains was adhered to the conductive tape and placed on the thin section. The quartz grains was dispersed and arranged, and then the gold conductive film was sprayed. The adhesive tape with quartz grains was placed in the sample cabin of scanning electron microscope, and then used different magnification to observe the micro morphology characteristics of quartz, and photos were taken for micro morphology statistics. During the observation process, the suspected grains were confirmed by energy spectra (Si-K characteristic single peak) to ensure that the statistical grains was quartz grains.

#### 3.2.2. Major Elements Analysis

The major elements were analyzed in ALS laboratory group (ALS Minerals–ALS Chemex) in Guangzhou, China. The analytical instrument was the Axios Max X-ray fluorescence spectrometer (XRF) produced by PANalytical company in Almelo, the Netherlands. Samples were dried and mixed with appropriate amount of lithium metaborate reagent in a porcelain crucible. The evenly mixed samples were melted in a high temperature melting furnace and made into glass melting pieces.

#### 3.2.3. Carbon and Oxygen Isotope Analysis

The carbon and oxygen isotope analyzed were also conducted in ALS laboratory group (ALS Minerals–ALS Chemex) in Guangzhou. Samples were crushed and sieved, and then, ground with a mortar to a pore size of 0.071 m (200 mesh) or less. Add concentrated phosphoric acid to the sample. Calcite in the sample reacts with concentrated phosphoric acid, and CO<sub>2</sub> is released after reaction at 72 °C for 4 h. Gas Bench and Delta Plus XP isotope mass spectrometer (CF-IRMS) are used to determine the values of  $\delta^{13}\text{C}$  (RSD < 0.03%, V-PDB standardization) and  $\delta^{18}\text{O}$  (RSD < 0.05%, V-SMOW standardization).

#### 3.2.4. Mossbauer Spectroscopy Analysis

The Mossbauer spectroscopy analysis was carried out in the Mossbauer spectrum laboratory of School of Physics and Technology, Wuhan University, Wuhan, China. The analytical instrument was Bench ms-500 produced by Wissel company, Starnberg, Germany. The radiation source was <sup>57</sup>Co and the intensity was 25 mci. Calculation result show that best mass of the sample to be analyzed was 150~250 mg in order to obtain a high-quality Mossbauer spectroscopy [16]. The samples were analyzed at low temperature (about 77 K) and room temperature (about 293 K), respectively. The Mossbauer data were analyzed by WinNoroms-for-Igor software.

## 4. Analysis Results

### 4.1. Micro Characteristics of Quartz Grains in Fault Gouge

Due to the low content of quartz in fault gouge of F<sub>4</sub> fault, it seems quite difficult to collect enough quartz grains for statistics. The micro characteristics of quartz grains are in fault gouge of F<sub>2</sub> and F<sub>7</sub>. According to the previous research results [10,17,18], the quartz micro morphology of the two faults is divided into type Ru, type Ia, type Ib, type Ic, type II, III and type IV in this study.

Most of the quartz grains in TMS01 are sub angular, and a small amount of quartz grains are irregular with obvious denudation pits on the surface. In addition to the weak-medium denudation micro morphology, a large number of subconchoidal and squamous-like micro morphology is developed. The quartz grains in TMS04 are mostly angular, with obvious denudation. Compared with TMS01, the number of orange peel and mossy-like

micro morphology increased significantly. The shape characteristics of TMS06 shows large amount of mossy and squamous-like micro morphology. The quartz grains in TMS07 mainly show weak denudation with subconchoidal and linear scratch, indicating a secondary deformation (Figure 3).

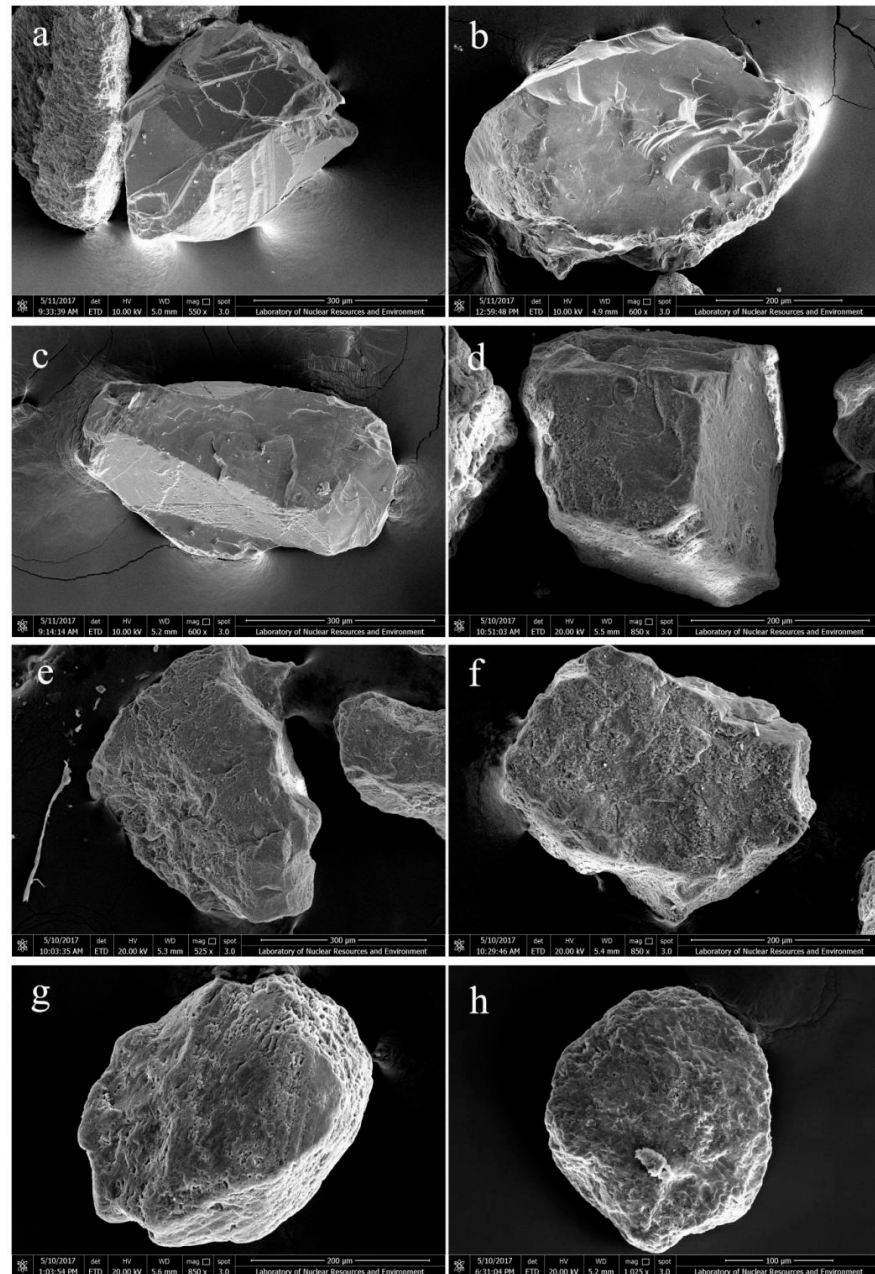


**Figure 3.** Typical quartz morphology in fault gouge from SEM. (a,b) angular grain, the surface is conchoidal fracture and straight crack (Ru type, TMS01); (c) subangular grain, the surface is subconchoidal fracture, local orange peel-like (Ia type, TMS04); (d) subangular grain, the surface is orange peel-like (Ib type, TMS07); (e) subangular grain, the surface is squamous-like (Ic type, TMS01); (f) subangular grain, the surface is mossy-like (II type, TMS01); (g) spheroid grain, the surface is worm hole-like (III type, TMS06); (h) globular grain, the surface is pothole and coral-like (IV type, TMS04).

#### 4.2. Characteristics of Major Elements in Fault Gouge and Host Rock

On the whole, major element contents in fault gouge and host rock of the same fault are similar, but different sampling points of the same fault are obviously different (Table S2).

In F<sub>2</sub> fault, TFe<sub>2</sub>O<sub>3</sub> and MgO are enriched in fault gouge, and BaO, MnO and SO<sub>3</sub> are relatively low. The characteristics of major elements in three locations of F<sub>7</sub> fault are different. The contents of TFe<sub>2</sub>O<sub>3</sub> and Na<sub>2</sub>O in fault gouge of the same sampling location are lower than those in host rock, and K<sub>2</sub>O is relatively enriched. The different in alumina, silica and total iron content may result from heterogeneity of the geological bodies. In F<sub>4</sub> fault, SiO<sub>2</sub>, Na<sub>2</sub>O and K<sub>2</sub>O in gouge samples are relatively low, while TFe<sub>2</sub>O<sub>3</sub> and SO<sub>3</sub> are higher. Compared with other samples, the loss-on-ignition of F<sub>4</sub> fault samples is higher.

#### 4.3. Carbon and Oxygen Isotope Characteristics of Fault Gouge and Host Rock

The δ<sup>13</sup>C and δ<sup>18</sup>O compositions of different fault samples are different (Table S3). The δ<sup>13</sup>C value of the F<sub>2</sub> and F<sub>7</sub> fault host rock whose lithology is mainly medium-coarse sandstone is −7.9‰~−4.1‰, and the δ<sup>18</sup>O value is 11.1‰~18.2‰. The δ<sup>13</sup>C value of the F<sub>4</sub> fault host rock whose lithology is mainly clay rock is 3.7‰, and the value of δ<sup>18</sup>O is 28.6‰. The δ<sup>13</sup>C and δ<sup>18</sup>O of three fault gouge samples of F<sub>7</sub> fault are −3.3‰~−5.9‰ and 9.0‰~14.9‰, respectively, the δ<sup>13</sup>C and δ<sup>18</sup>O of two host rock samples are −4.1‰~−6.1‰ and 11.1‰~13.7‰, respectively. During the experiment, the carbon and oxygen isotope of TMS01 could not be analyzed because of the low carbonate content.

#### 4.4. Mossbauer Spectroscopy Characteristics of Fault Gouge and Host Rock

Samples were analyzed at room temperature (about 293 K) and low temperature (77 K), respectively (Table S4). Because less Mossbauer nuclei in the sample will lead to the weaker intensity, and it is difficult to obtain accurate Mossbauer parameters [16]; lower the analyzed temperature can enhance the Mossbauer effect [19]. Therefore, in order to obtain high quality Mossbauer spectra, TMS01 and TMS02 samples were selected and analyzed at low temperature (77 K).

Distribution characteristics of iron species in fault gouge and host rock samples of three faults can be obtained (Figure S1 and Figure 4). F<sub>2</sub> fault gouge show two doublets at room temperature, indicating that there are two kinds of iron species, and it is paramagnetic iron. The addition of two sextets at low temperature indicates existence of the super fine magnetic grain. The spectra distributions are similar between host rock and the gouge, suggesting they are homologous. Compared with the host rock, F<sub>4</sub> fault gouge has a doublets (para-Fe<sup>3+</sup>), indicating that the iron species of fault gouge and surrounding rock is different. F<sub>7</sub> fault gouge and host rock only contain three doublets, and the peak shape is similar, indicating that the iron species of both is consistent and relatively stable.

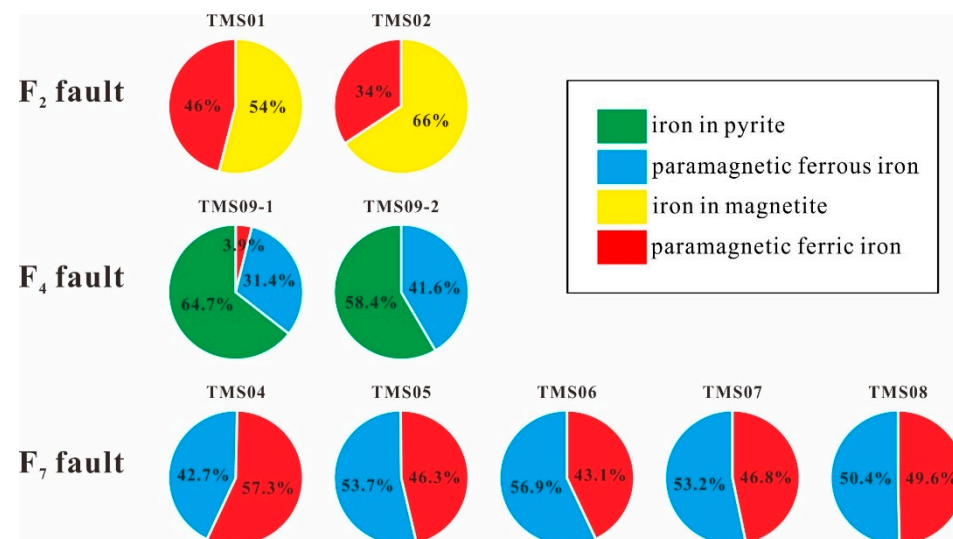


Figure 4. Relative content of iron species in fault gouge and host rock in the Tamusu area.

## 5. Discussion

### 5.1. Micro Characteristics of Quartz Grains

Fresh surface of quartz grains will appear typical conchoidal fracture, crack and other stress trace micro morphology, namely Ru. When the fault stopped activity, the surface of quartz grains in fault gouge was denudation, and with the increase of dissolution time, it showed subconchoidal to coral-like structure [20]. Kanaori classified the denudation morphology of quartz grains into four types according to the observation results on SEM: type I, type II, type III and type IV, and studied the chronology of quartz grains with these four denudation morphology characteristics [10]. Type I micro morphology can be further subdivided into Ia, Ib and Ic [18]. Classification of micro topography and the relative age of its formation are illustrated (Table S5).

From the micro morphology characteristics of different types of quartz, with the strengthening of denudation, the micro morphology of quartz denudation has obvious progressive changes. For example, the sharp edges and ridges of quartz grains gradually disappear, the flat and smooth surface become more and more rough and uneven, and the size and depth of the denudation hole increase and deepen. Statistically, the distribution characteristics of different types of micro morphology of quartz grains in fault gouge of F<sub>2</sub> and F<sub>7</sub> are obtained (Figure 5). By comparing the SEM characteristics of quartz grains in fault gouge with Table S5, the relative formation age of surface micro characteristics of quartz grains can be inferred (Table S6).

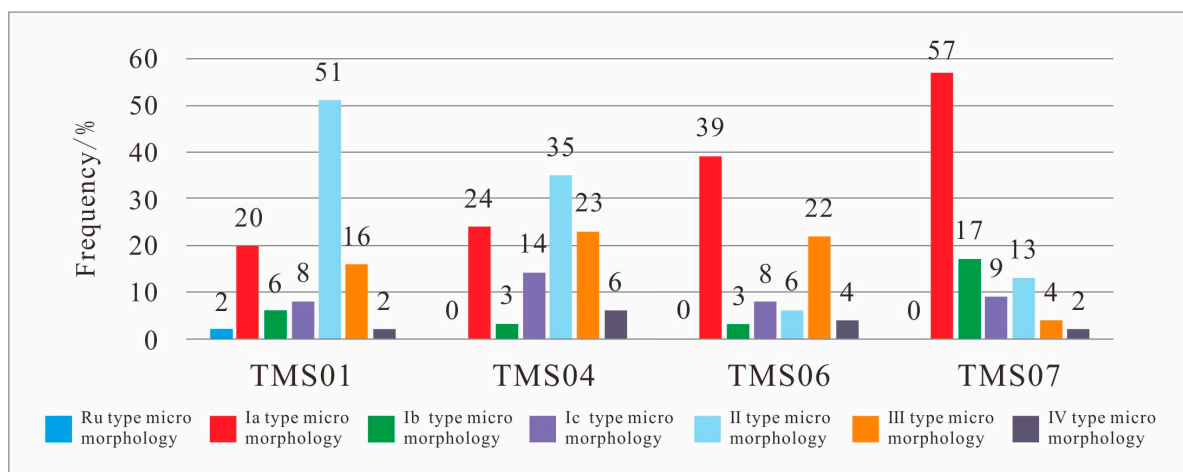


**Figure 5.** Classification and frequency of micro morphology of quartz grains in fault gouge.

The quartz micro morphology in TMS01 samples collected from F<sub>2</sub> fault is mainly of type Ia, type II and III, indicating that the activity age of F<sub>2</sub> is mainly in late Pleistocene, early Pleistocene and Pliocene. Besides, in the overall change of quartz micro morphology frequency from F<sub>2</sub>, it first increases, then decreases, then increases and then decreases, the two peaks of quartz micro morphology frequency are type Ia and type II. It suggests that the F<sub>2</sub> fault may have two stages of activity, probably in the early Pleistocene and late Pleistocene. The type II micro morphology accounts for the highest proportion, which indicates that the activity intensity of the fault in the early Pleistocene is greater than that in the late Pleistocene.

The quartz micro morphology in TMS04 collected from F<sub>7</sub> is mainly of type Ia, type Ic, type II and type III, indicating that the fault is active in late Pleistocene, early Pleistocene and Pliocene; To the TMS06, it is mainly of type Ia and type III, indicating that the fault is active in late Pleistocene and Pliocene; and the TMS07 is mainly of type Ia, type Ib, type Ic and type II with an active ages probably late Pleistocene, middle Pleistocene and early Pleistocene. The quartz micro morphology of fault gouge samples from different sampling locations of F<sub>7</sub> indicates pulsing activity. On the whole, the main active periods

are late Pleistocene, early Pleistocene and Pliocene, which suggests that the fault activity had continuance and began from Pliocene. From the overall distribution of quartz micro morphology of the three samples from F<sub>7</sub>, the proportion of type Ia is the highest, which indicates that the activity intensity of late Pleistocene is higher than others. The type of Ru in all samples is almost zero in F<sub>2</sub> and F<sub>7</sub>, which indicates that the two faults are basically inactive since Holocene.

### 5.2. Major Elements

The migration of fluid and its participation in fluid-rock interaction will inevitably change the chemical composition of fault zone. The active elements would be carried away by the fluid, while the relatively stable elements remain in the fault zone [21–23]. Previous study results show that there is a good consistency between the variation of elements and minerals in the fault zone of different protoliths, and the elements related to feldspar are mainly lost in the fault zone of hosting clastic sedimentary rock and crystalline rock series [24,25]. The study of core in Nojima fault zone shows that SiO<sub>2</sub>, K<sub>2</sub>O, Na<sub>2</sub>O, Rb and Pb in the fault zone are greatly depleted, and some high field strength elements are enriched [26,27]. Study of several fault sections on the surface of Andreas fault zone also shows that the elements lost mainly include Na<sub>2</sub>O, Al<sub>2</sub>O<sub>3</sub>, SiO<sub>2</sub> and K<sub>2</sub>O related to feldspar [21,28]. TiO<sub>2</sub>, P<sub>2</sub>O<sub>5</sub> and MnO are generally considered as stable elements [29]. Therefore, the degree of fluid-rock interaction in the fault zone can be indicated by the enrichment of stable elements and the depletion of active elements, and the degree of fluid-rock interaction in the fault zone is closely related to the intensity of fault activity [6–8].

In F<sub>2</sub>, TFe<sub>2</sub>O<sub>3</sub> and MgO are relatively enriched, while the enrichment and depletion of other elements are not obvious, indicating that the degree of fluid-rock interaction in the fault zone is low and the intensity of fault activity is weak. The enrichment of TFe<sub>2</sub>O<sub>3</sub> and MgO may be related to the introduction of Fe and Mg in the meteoric fluid, which indicates that the F<sub>2</sub> fault is characterized by shallow activity.

In F<sub>4</sub>, TFe<sub>2</sub>O<sub>3</sub>, SO<sub>3</sub>, CaO, BaO and SrO are relatively enriched, while SiO<sub>2</sub>, K<sub>2</sub>O and Na<sub>2</sub>O are relatively low. The enrichment of SO<sub>3</sub> and CaO may be related to pyrite and carbonate minerals involved in fault activity. The weak depletion of SiO<sub>2</sub>, K<sub>2</sub>O and Na<sub>2</sub>O indicates the weak fluid-rock interaction in the fault zone.

The element contents from different sampling locations of F<sub>7</sub> have obvious differences. In the TMS04, TFe<sub>2</sub>O<sub>3</sub>, MgO and Na<sub>2</sub>O are depleted, while SiO<sub>2</sub> and K<sub>2</sub>O are enriched, which indicates that the fluid-rock interaction in fault zone is strong. All the elements in TMS07 show no obvious depletion and enrichment, which indicates that the fluid-rock interaction in the fault zone is weak, and the intensity of fault activity is low. In addition, the contents of major elements in fault gouges of TMS04, TMS06 and TMS07 are also quite different. The difference of element distribution in different sampling sites of F<sub>7</sub> fault shows the pulsing activity of fault, and the intensity of fault activity is also different.

### 5.3. Carbon and Oxygen Isotope Characteristics and Their Implications

The isotope composition of fault rocks will also change due to the process of fluid leaching and fluid-rock interaction during the fault activity. Stable isotope ( $\delta^{13}\text{C}$ ,  $\delta^{18}\text{O}$ ) geochemistry can provide basic information of fluid source and water rock interaction [30–32]. There are three main sources of carbon in carbonate minerals in normal fault gouge: (1) marine carbonate with average value of  $\delta^{13}\text{C}_{\text{PDB}}$  about 0‰ [33,34]; (2) the  $\delta^{13}\text{C}_{\text{PDB}}$  of organic carbon in rocks ranges from  $-30\text{‰}$ ~ $-15\text{‰}$ , with an average of  $-22\text{‰}$  [30,33]; (3) deep source carbon that includes magma and mantle-derived gas with  $\delta^{13}\text{C}_{\text{PDB}}$  range of  $-9\text{‰}$ ~ $-3\text{‰}$  and  $-5\text{‰}$ ~ $-2\text{‰}$  [35]. The carbon and oxygen isotope of many active fault zones have been studied by predecessors.  $\delta^{18}\text{O}$  values of carbonate minerals in the San Andreas fault from  $15\text{‰}$ ~ $25\text{‰}$ , and the  $\delta^{13}\text{C}$  values range from  $-7\text{‰}$ ~ $5\text{‰}$ . The variation values generally show a decreasing trend from the host rock to the fault zone, indicating that the fluid interaction to the fault core is gradually enhanced [31]. The analysis of carbonate matrix, vein and breccia samples in Wenchuan fault zone shows that the  $\delta^{18}\text{O}$  values

of matrix and vein are 19‰~21‰, and breccia is 19.6‰~28‰. The  $\delta^{13}\text{C}$  values of veins are  $-8\text{‰} \sim -4.5\text{‰}$  and breccia are  $-3.7\text{‰} \sim -1.6\text{‰}$ . The large breccia grains have similar isotope compositions to the host rocks, indicating that they have less interaction with the fluid, while the matrix and vein were more interactive with the fluid and have more depleted isotope compositions [36]. The analysis of the vein samples from Tiantaichang and Daershan fault zone in Jiaoshiba anticline shows that the  $\delta^{18}\text{O}$  values of the veins are 17.2‰~26.8‰ and the  $\delta^{13}\text{C}$  values are between  $-4.7\text{‰} \sim 4.5\text{‰}$ . Combined with the strontium isotope values of the samples, show that they are affected by the deep thermal fluid, and the vertical sealing of the fault is poor [23].

The  $\delta^{13}\text{C}_{\text{PDB}}-\delta^{18}\text{O}_{\text{SMOW}}$  diagram shows a nearly horizontal distribution of carbon and oxygen isotope of the three fracture samples (Figure 6). This isotopic distribution may be caused for two reasons: (1)  $\text{CO}_2$  degassing; (2) fluid-rock interaction between fluid and host rock [37,38]. In the inactive fault with good sealing property, the fluid from the host rock has enough time to exchange carbon and oxygen isotope with the host rock to reach the balance, which makes the  $\Delta\delta^{13}\text{C}$  and  $\Delta\delta^{18}\text{O}$  between the fault gouge and the host rock closer. According to Table S4 and Figure 6, it can be inferred that:

The  $\delta^{13}\text{C}$  and  $\delta^{18}\text{O}$  values of fault gouge in  $F_4$  fault are  $-0.2\text{‰}$  and 22.1‰ respectively, in host rock are 3.7‰ and 28.6‰. The  $\delta^{18}\text{O}$  of fault gouge is lower than host rock due to the influence of atmospheric precipitation in the fault zone, indicating the fault barely has a link to deep fluid [39]. The CaO of the two samples are 12% and 19%, respectively. Combined with the isotope characteristics of the samples, it indicates that the carbonates in the strata are not primary and may be related to the underlying Paleozoic marine sedimentary rocks [33].

The  $\delta^{13}\text{C}$  values of TMS04, TMS05 and TMS06 at the same sampling point of  $F_7$  fault are  $-3.3\text{‰}$ ,  $-4.1\text{‰}$  and  $-4.8\text{‰}$ , respectively. The difference is not significant among the three samples, and the  $\delta^{18}\text{O}$  values are similar, but the  $\delta^{18}\text{O}$  value of host rock is slightly higher, indicating that the fluid in the fault zone mainly comes from the host rock. The isotope characteristics of gouge and host rock may be influenced by low temperature hydrothermal. It is speculated that the deep hydrothermal migrated along the fault to the shallow location and mixed with meteoric water. All the samples show the characteristics of carbon and oxygen isotope balance, indicates that the fault is well sealed and the activity is low. In addition, the difference of fluid properties in different sampling locations may be related to the multi-stage activity of faults.

The carbonate in fault gouge TMS01 of  $F_2$  fault is too low to detect its carbon and oxygen isotope composition, making it impossible to determine the source of fluid involved in fault activity. CaO is highly active and varies greatly in the fault zone [30,40]. The content of CaO is low in the analyzed samples. It should be noted that meteoric water may dissolve, and took away most of the carbonate in fault gouge, indicating that the fault has connectivity with the shallow, but poor connectivity with deep part.

#### 5.4. Fe Species

Iron is a redox sensitive element. In the deep part of an active fault, there are often reducing fluids migrating up the fault, which leads to the reduction of iron in the shallow fault gouge. The Ushikubi fault zone in central Japan illustrated ferric oxide and reduced iron in the old and new faults, respectively, indicating these redox shifts probably relate to the material exchange between the fault gouge and the external or deep [42]. Ma Xiangxian studied the iron species of fresh fault gouge in Wenchuan fault zone which had an 8.0 earthquake magnitude in 2008 and found that the fault gouge is mainly enriched with reduced Fe, it is resulted from exchange with deep reducing materials and suggest it a typical active fault [43].

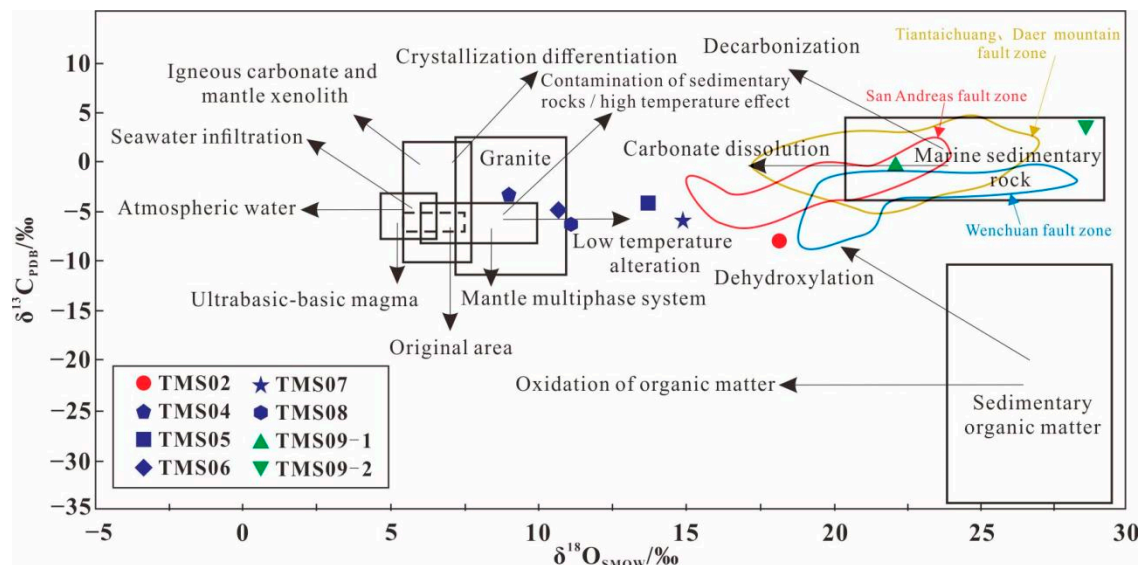


Figure 6. Carbon and oxygen isotopic characteristics of fault gouge and host rock in the Tamusu area [41].

The faults in and around the Tamusu site candidate is compressive-torsional faults, that make these faults formed a relative closed system [44]. Mossbauer spectroscopy results show that only oxidized iron is detected in fault gouge and host rock of F<sub>2</sub> fault, of which para-Fe<sup>3+</sup> comes from clay mineral with relative content of 46%, and mag-Fe<sup>3+</sup> probably be iron in maghemite with relative content of 54%. It indicates that the environment of F<sub>2</sub> is strong oxidized environment. The iron content in fault gouge (2.47 wt%) is much higher than that in host rock (0.52 wt%). The solubility of Fe is very low, especially Fe<sup>3+</sup> can hardly be transported. The enrichment of oxidizing iron in fault zone can only be carried to the fault zone by easily soluble Fe<sup>2+</sup> to be oxidized and then precipitated [45], which makes the environmental condition of fault zone change from reduction to oxidation condition. Comprehensively, the sealing of F<sub>2</sub> fault is very good with very poor connectivity to the deep.

The iron species in the host rock of F<sub>4</sub> are all ferrous iron, whereas the fault gouge contain small amount of oxidized iron which is contributed by clay minerals. The clay content reaches 52% in the fault gouge [46]. Distribution characteristics of iron species show that the fault zone gradually tends to open due to the attenuation of compressive stress during the evolution of the fault, and the environment where the fault is located begins to transition from reducing environment to oxidizing environment. Fault gouge continuously fills in the fissure of the fault zone, and the fault zone gradually tends to be closed, reducing the connectivity with the outside world, and only a small amount of reductive iron is oxidized.

The F<sub>7</sub> fault samples show that the content of oxidized and reduced iron in fault gouge and host rock is almost the same. Both para-Fe<sup>3+</sup> and para-Fe<sup>2+</sup> are contributed by clay minerals. X-ray powder diffraction results shows that the content of clay minerals is 38–87% [46]. The samples were collected from an artificial blasting outcrop. The distribution characteristics of iron species show that the exchange between the fault zone and the deep reducing fluid is weak, and the increase of the proportion of oxidized iron needs a long time of material exchange with the outside world. F<sub>7</sub> fault is a large concealed fault, which is overlaid by the upper Cretaceous and Quaternary strata, and the precipitation and aggregation of new minerals in the fault zone will reduce the connectivity with the deep underground, making the fault zone in a relatively “closed” state [47,48]. Combined with major elements feature and iron species, a conceptual diagram has been proposed (Figure 7).

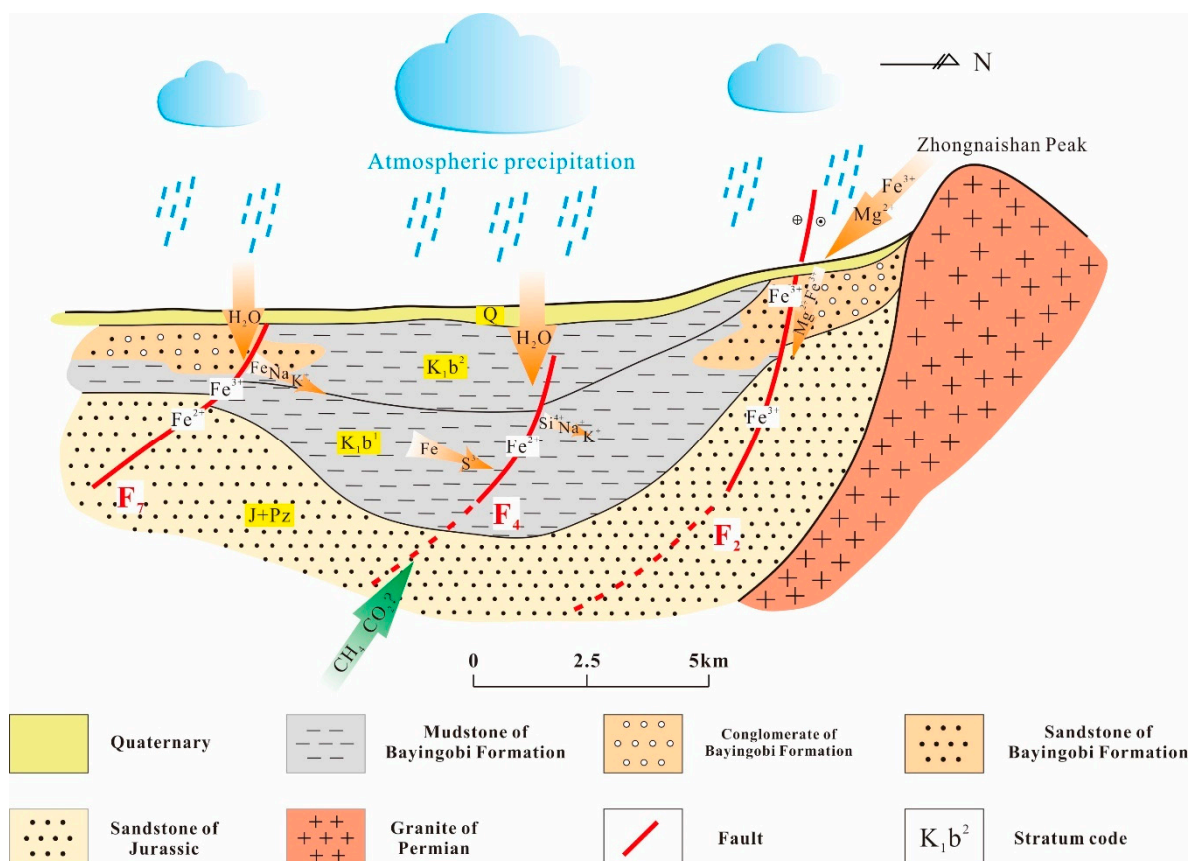


Figure 7. Conceptual diagram showing the features of the three study faults.

## 6. Conclusions

Three faults in the site candidate were studied, and the result show that the faults illustrated weak connection with the deep, indicating they are stable, and it is a favorable area to be a site candidate for the geological repository of HLW. However, individual fault has features that should be noted.

(1)  $F_2$  fault is characterized by the enrichment of oxidized iron, and the content of CaO in the fault gouge with strong activity is low, indicating that the fault activity may be weak, with poor connectivity with the deep. Except for Fe and Mg, the enrichment and depletion of other major elements are not obvious, indicating that the degree of fluid-rock interaction is low. Due to the low carbonate content of fault gouge sample TMS01, it is impossible to determine the source of fluid involved in fluid-rock interaction by carbon and oxygen isotopes. Micro features of quartz grains show that  $F_2$  fault may have two periods of activity, mainly in the early Pleistocene and late Pleistocene.

(2) The iron species in the fault gouge of  $F_4$  fault show that the pyr- $Fe^{2+}$  in the fault zone is relative high, indicating a weak reduction environment, which is consistent with weak depletion of Si, K, Na and enrichment of S, Fe and Ca. The carbon and oxygen isotopic compositions of wall rock and fault gouge are different, indicating that the fault has experienced fluid-rock reaction. The  $\delta^{18}O$  of the host rock is slightly higher, which may be due to the influence of meteoric water. Attention should be paid to induced earthquake risk.

(3)  $F_7$  fault is a concealed fault with weak connectivity to the surface in the site candidate area. The fault illustrated multi-stage activities by micro features of quartz grains and carbon and oxygen isotopic compositions, its activity is weak since Holocene.

Comprehensively, part of the  $F_4$  fault is located in the site candidate, and the occurrence of a small amount of pyrite in the fault zone and the difference of carbon and oxygen isotopes indicate that it may experience material exchange with the deep zone. Moreover,

the content of clay minerals in the F<sub>4</sub> and F<sub>7</sub> faults is high. Therefore, attention should be paid to the activity of the F<sub>4</sub> fault and the possibility of the two faults to induce earthquakes.

**Supplementary Materials:** The following are available online at <https://www.mdpi.com/article/10.3390/min11090941/s1>, Figure S1: Mossbauer spectroscopy of fault gouge and host rock in Tamusu area. Table S1: Sample characteristics and sampling location. Table S2: Major element content in fault gouge and host rock. Table S3: Carbon and oxygen isotope compositions of fault gouge and host rock. Table S4: Mossbauer parameters and relative contents of various iron species in fault samples from Tamusu area. Table S5: Micro morphological classification and relative chronology of quartz in fault gouge. Table S6: Micro morphology type and formation age of quartz grains in fault gouge.

**Author Contributions:** Conceptualization, Z.R. and G.L.; methodology, Z.R., X.L. and G.L.; investigation, X.L., P.L., H.L., S.L., M.Z., C.G., F.N., Z.G. and F.A.; data curation, Z.R., C.G. and F.N.; writing—original draft preparation, Z.R., writing—review and editing, G.L. and X.L.; project administration, X.L., P.L. and G.L. All authors have read and agreed to the published version of the manuscript.

**Funding:** This work was funded by the National Defense science, Technology and Industry Bureau project (NO. (2014) 1587), Independent Fund Projects from the State Key Laboratory of Nuclear Resources and Environment (No. Z1904), and Jiangxi Special Development Fund of Centre-guide-local (No. 2018ZDB40001).

**Data Availability Statement:** Some of the data presented in this study are available in the Supplementary Materials, Figure S1 and Tables S1–S6.

**Acknowledgments:** We would like to express sincere thanks to Shuiwei Zhao from China Institute for Radiation Protection and Miles Silberman from the University of Texas at El Paso are acknowledged for their helpful comments.

**Conflicts of Interest:** The authors declare no conflict of interest.

## References

1. IAEA. Geological Disposal of Radioactive Waste: Technological Implications for Retrievability, NW-T-1.19. 2009. Available online: <https://www.iaea.org/publications/8022/geological-disposal-of-radioactive-waste-technological-implications-for-retrievability> (accessed on 21 August 2021).
2. Wang, C.X.; Liu, X.D.; Liu, P.H. The general situation of clay site for high-level waste geological disposal repository. *Radiat. Prot.* **2008**, *28*, 310–316.
3. Yuan, G.; Zhang, L.; Zeng, Q.; Huang, Z.; Li, J.; Wang, H.; Deng, X. Prediction of rock mass quality in target depth for Tamusu area of Alxa pre-selected region for geological disposal of high-level nuclear waste. *J. Eng. Geol.* **2018**, *26*, 1690–1700. (In Chinese)
4. Wintsch, R.P.; Christoffersen, R.; Kronenberg, A.K. Fluid-rock reaction weakening of fault zones. *J. Geophys. Res. Solid Earth* **1995**, *100*, 13021–13032. [[CrossRef](#)]
5. Zheng, G.D. Iron Speciation by Mössbauer Spectroscopy and Its Implications in Various Studies on the Earth Surface Processes. *Bull. Mineral. Petrol. Geochem.* **2008**, *27*, 161–168.
6. Sibson, R.H.; Moore, J.M.M.; Rankin, A.H. Seismic pumping—A hydrothermal fluid transport mechanism. *J. Geol. Soc.* **1975**, *131*, 653–659. [[CrossRef](#)]
7. Sibson, R.H. Implications of fault-ave behavior for rupture nucleation and recurrence. *Tectonophysics* **1992**, *211*, 283–293. [[CrossRef](#)]
8. Sinisi, R.; Petrucci, A.V.; Agosta, F.; Paternoster, M.; Belviso, C.; Grassa, F. Contrasting fault fluids along high-angle faults: A case study from Southern Apennines (Italy). *Tectonophysics* **2016**, *690*, 206–218. [[CrossRef](#)]
9. Boles, A.; Mulch, A.; Ben VD, P. Near-surface clay authigenesis in exhumed fault rock of the Alpine Fault Zone (New Zealand); O-H-Ar isotopic, XRD and chemical analysis of illite and chlorite. *J. Struct. Geol.* **2018**, *111*, 27–41. [[CrossRef](#)]
10. Kanaori, Y.; Kazuhiro, T.; Katsuyoshi, M. Further studies on the use of Quartz grain from fault gouges establish the age of faulting. *Eng. Geol.* **1985**, *21*, 175–194. [[CrossRef](#)]
11. Niwa, M.; Shimada, K.; Aoki, K.; Ishimaru, T. Microscopic features of quartz and clay particles from fault gouges and infilled fractures in granite: Discriminating between active and inactive faulting. *Eng. Geol.* **2016**, *210*, 180–196. [[CrossRef](#)]
12. Wiseall, A.C.; Cuss, R.J.; Hough, E.; Kemp, S.J. The role of fault gouge properties on fault reactivation during hydraulic stimulation; an experimental study using analogue faults. *J. Nat. Gas Sci. Eng.* **2018**, *59*, 21–34. [[CrossRef](#)]
13. Guan, W.C.; Liu, X.D.; Liu, P.H. Study on the geological characteristics of claystone in Tamusu area of Bayingebi basin. *World Nucl. Geosci.* **2014**, *31*, 95–102. (In Chinese)
14. Zhang, C.Y.; Nie, F.J.; Hou, S.R.; Wang, J.L.; Deng, W.; Zhang, L. Tectonic evolution characteristics of Bayingebi basin and its control on the mineralization of sandstone type uranium deposits. *Uranium Geol.* **2015**, *31*, 384–388. (In Chinese)

15. Chen, G.; Shi, J.; Jiang, T.; Zhang, H.; Li, W.; Wang, B. LA-ICP-MS zircon U-Pb dating and geochemistry of granitoids in Tamusu, Alxa Right Banner, Inner Mongolia. *Geol. Bull. China* **2015**, *34*, 1884–1896. (In Chinese)
16. Zhang, F.L.; Yi, F.; Chen, Y.L.; Xu, F. Determination of the optimum thickness of an absorber in Mössbauer spectroscopy. *J. Wuhan Univ. (Nat. Sci. Ed.)* **1997**, *43*, 348–352. (In Chinese)
17. Kanaori, Y.; Miyakoshi, K.; Kakuta, T.; Satake, Y. Dating fault activity by surface textures of quartz grains from fault gouges. *Eng. Geol.* **1980**, *16*, 243–262. [[CrossRef](#)]
18. Shen, J.; Yang, W.; Liu, T.; Huang, X.; Zheng, W.; Wang, G.; Yu, L. Micro-morphology of quartz in the Bailong river fault gouge, west Qinling, China, and its chronological significance. *Bull. Mineral. Petrol. Geochem.* **2014**, *33*, 271–278. (In Chinese)
19. Zhang, J.; Yin, Y.; Zhang, Y.; Ma, L. Mössbauer apparatus—A powerful characterization technique. *Mod. Instrum. Med. Treat.* **2003**, *9*, 33–36.
20. Kanaori, Y. A SEM cathodoluminescence study of quartz in mildly deformed granite from the region of the Atotsugawa fault, central Japan. *Tectonophysics* **1986**, *131*, 133–146. [[CrossRef](#)]
21. Goddard, J.V.; Evans, J.P. Chemical Changes and Fluid-Rock Interaction in Faults of Crystalline Thrust Sheets, Northwestern Wyoming, U.S.A. *J. Struct. Geol.* **1995**, *17*, 533–547. [[CrossRef](#)]
22. Chen WM, D.; Tanaka, H.; Huang, H.J.; Lu, C.B.; Lee, C.Y.; Wang, C.Y. Fluid infiltration associated with seismic faulting: Examining chemical and mineralogical compositions of fault rocks from the active Chelungpu fault. *Tectonophysics* **2007**, *443*, 243–254. [[CrossRef](#)]
23. Chen, J.; Yang, X.; Ma, S.; Spiers, C.J. Mass removal and clay mineral dehydration/rehydration in carbonate-rich surface exposures of the 2008 Wenchuan Earthquake fault: Geochemical evidence and implications for fault zone evolution and coseismic slip. *J. Geophys. Res. Solid Earth* **2013**, *118*, 474–496. [[CrossRef](#)]
24. Isaacs, A.J.; Evans, J.P.; Sheng-Rong, S.; Kolesar, P.T. Structural, Mineralogical, and Geochemical Characterization of the Chelungpu Thrust Fault, Taiwan. *Terr. Atmos. Ocean. Ence* **2007**, *18*, 183–221. [[CrossRef](#)]
25. Schleicher, A.M.; Tourscher, S.N.; van der Pluijm, B.A.; Warr, L.N. Constraints on mineralization, fluid-rock interaction, and mass transfer during faulting at 2–3 km depth from the SAFOD drill hole. *J. Geophys. Res. Solid Earth* **2009**, *114*, B04202. [[CrossRef](#)]
26. Tanaka, H.; Fujimoto, K.; Ohtani, T.; Ito, H. Structural and chemical characterization of shear zones in the freshly activated Nojima fault, Awaji Island, southwest Japan. *J. Geophys. Res. Solid Earth* **2001**, *106*, 8789–8810. [[CrossRef](#)]
27. Matsuda, T.; Omura, K.; Ikeda, R.; Arai, T.; Kobayashi, K.; Still, K.; Tanaka, H.; Saw, T.I.; Hirano, S. Fracture-zone conditions on a recently active fault: Insights from mineralogical and geochemical analyses of the Hirabayashi NIED drill core on the Nojima fault, southwest Japan, which ruptured in the 1995 Kobe earthquake. *Tectonophysics* **2004**, *378*, 143–163. [[CrossRef](#)]
28. Evans, J.P.; Chester, F.M. Fluid-rock interaction in faults of the San Andreas system: Inferences from San Gabriel fault rock geochemistry and microstructures. *J. Geophys. Res.* **1995**, *100*, 13007–13013. [[CrossRef](#)]
29. Duan, Q.B.; Yang, X.S.; Chen, J.Y. Review of geochemical and petrophysical responses to fluid processes within seismogenic fault zones. *Prog. Geophys.* **2015**, *30*, 2448–2462. (In Chinese)
30. Kirschner, D.L.; Kennedy, L.A. Limited syntectonic fluid flow in carbonate-hosted thrust faults of the Front Ranges, Canadian Rockies, inferred from stable isotope data and structures. *J. Geophys. Res. Solid Earth* **2001**, *106*, 8827–8840. [[CrossRef](#)]
31. Pili, É.; Poitrasson, F.; Gratier, J.P. Carbon–oxygen isotope and trace element constraints on how fluids percolate faulted limestones from the San Andreas Fault system: Partitioning of fluid sources and pathways. *Chem. Geol.* **2002**, *190*, 231–250. [[CrossRef](#)]
32. Pili, É.; Kennedy, B.M.; Conrad, M.E.; Gratier, J.P. Isotopic evidence for the infiltration of mantle and metamorphic CO<sub>2</sub>-H<sub>2</sub>O fluids from below in faulted rocks from the San Andreas Fault system. *Chem. Geol.* **2011**, *281*, 242–252. [[CrossRef](#)]
33. Veizer, J.; Holser, W.T.; Wilgus, C.K. Correlation of 13C/12C and 34S/32S secular variations. *Geochim. Cosmochim. Acta* **1980**, *44*, 579–587. [[CrossRef](#)]
34. Ohmoto, H. Systematics of Sulfur and Carbon Isotopes in Hydrothermal Ore Deposits. *Econ. Geol.* **1972**, *67*, 551–578. [[CrossRef](#)]
35. Taylor, B.E. Magmatic volatiles; isotopic variation of C, H, and S. *Rev. Mineral. Geochem.* **1986**, *16*, 185–225.
36. Guo, J.; Yan, X.; Zihong, L.I.; Chen, H.; Guirang, H.U. Carbon and oxygen isotope fractionation of carbonate rocks in the fault zone of Wenchuan earthquake: Implications for the mechanism of fault healing. *Geol. Bull. China* **2019**, *38*, 959–966. (In Chinese)
37. Zheng, Y.F. Carbon-oxygen isotopic covariations in hydrothermal calcites during degassing of CO<sub>2</sub>, a quantitative evaluation and application to the Kushikino gold mining area in Japan. *Miner. Depos.* **1990**, *25*, 246–250. [[CrossRef](#)]
38. Zheng, Y.F.; Hoefs, J. Carbon and oxygen isotopic covariations in hydrothermal calcites. *Miner. Depos.* **1993**, *28*, 79–89. [[CrossRef](#)]
39. Kerich, R.; Tour, T.; Willmore, L. Fluid participation in deep fault zones: Evidence from geological, geochemical, and 18O/16O relations. *J. Geophys. Res. Solid Earth* **1984**, *89*, 4331–4343. [[CrossRef](#)]
40. Wang, P.L.; Wu, J.J.; Yeh, E.C.; Song, S.R.; Chen, Y.G.; Lin, L.H. Isotopic constraints of vein carbonates on fluid sources and processes associated with the ongoing brittle deformation within the accretionary wedge of Taiwan. *Terra Nova* **2010**, *22*, 251–256. [[CrossRef](#)]
41. Liu, J.J.; He, M.Q.; Li, Z.M. Oxygen and Carbon Isotopic Geochemistry of Baiyangping Silver-Copper Polymetallic Ore Concentration Area in Lanping Basin of Yunnan Province and Its Significance. *Miner. Depos.* **2004**, *23*, 1–10. (In Chinese)
42. Zheng, G.D.; Fu, B.H.; Takahashi, Y.; Miyahara, M.; Kuno, A.; Matsuo, M.; Miyashita, Y. Iron speciation in fault gouge from the Ushikubi fault zone central Japan. *Hyperfine Interact.* **2008**, *186*, 39–52. [[CrossRef](#)]
43. Ma, X.; Wang, H.; Zhang, Z.; Shi, P.; Zhao, J.; Zhang, H.; Song, Z. Distribution characteristics of iron species in three faults along the eastern margin of the Tibetan, China. *Bull. Mineral. Petrol. Geochem.* **2014**, *33*, 348–354. (In Chinese)

44. Harding, T.P.; Tuminas, A.C. Structural interpretation of hydrocarbon traps sealed by basement normal block faults at stable flank of foredeep basins and at rift basins. *AAPG Bull.* **1989**, *73*, 812–840.
45. Yang, W.M.; Huang, W.H. The characteristics of tectonic geochemistry of the fault zones on the southern and northern edges of Huainan coalfield, Anhui province. *Geoscience* **2002**, *16*, 251–256.
46. Guo, C.; Li, G.; Wang, Z.; Zhang, W.; Liu, S.; Gong, Z.; Liu, X. Distribution of Iron Species in Faults and Its Indication of Fault Activity in Tamusu Area, Inner Mongolia. *Geol. Rev.* **2018**, *64*, 1365–1378. (In Chinese)
47. Gudmundsson, A. Active fault zones and groundwater flow. *Geophys. Res. Lett.* **2000**, *27*, 2993–2996. [[CrossRef](#)]
48. Gudmundsson, A.; Berg, S.S.; Lyslo, K.B.; Skurtveit, E. Fracture networks and fluid transport in active fault zones. *J. Struct. Geol.* **2001**, *23*, 343–353. [[CrossRef](#)]